IOP Publishing Journal of Physics: Condensed Matter

J. Phys.: Condens. Matter **27** (2015) 105102 (7pp) doi:10.1088/0953-8984/27/10/105102

Friction and universal contact area law for randomly rough viscoelastic contacts

M Scaraggi[1,2] **and B N J Persson**[2]

[1] DII, Universitá del Salento, 73100 Monteroni-Lecce, Italy
[2] PGI, FZ-Jülich, 52425 Jülich, Germany

E-mail: michele.scaraggi@unisalento.it and b.persson@fz-juelich.de

Received 28 September 2014, revised 7 January 2015
Accepted for publication 8 January 2015
Published 9 February 2015

Abstract

We present accurate numerical results for the friction force and the contact area for a viscoelastic solid (rubber) in sliding contact with hard, randomly rough substrates. The rough surfaces are self-affine fractal with roughness over several decades in length scales. We calculate the contribution to the friction from the pulsating deformations induced by the substrate asperities. We also calculate how the area of real contact, $A(v, p)$, depends on the sliding speed v and on the nominal contact pressure p, and we show how the contact area for any sliding speed can be obtained from a universal master curve $A(p)$. The numerical results are found to be in good agreement with the predictions of an analytical contact mechanics theory.

Keywords: rubber friction, random roughness, contact area

(Some figures may appear in colour only in the online journal)

1. Introduction

Viscoelastic solids, such as rubber or gel, have many important applications in science and technology. Rubber friction, for example, is a topic of great practical importance e.g. for tires, syringes, wiper blades or rubber seals, and it results from dissipative processes involving multiple (coupled) nano- to micro- (or more) length scales, which are related to the relaxation and diffusion dynamics of the confined polymers [1–4] as well as to the random interaction process [5] occurring in real interfaces. Due to the (numerical) complexity of the underlying contact mechanics problem [6–9], involving multiple length and time scales, the friction force as well as the real contact area between viscoelastic solids under *realistic* contact conditions has so far only been predicted using mean field formulations of the contact mechanics, such as the one by Persson [5] or Klüppel and Heinrich [10]. Comparing theory with experimental results is an important benchmark for any theory validation process, but the superposition of coupled dissipation mechanisms encountered in rubber friction makes it very hard to test separately the different contributions to the rubber friction. Hence, in this context any numerically-exact calculations under well defined contact characteristics, even if only possible for relatively-small systems under idealized conditions, can furnish very useful insights into the processes occurring in rubber sliding contacts, and test analytical theories.

In this work we make an attempt to shed light on the mechanisms of micro-rolling friction and contact area formation in the interaction between randomly rough surfaces of viscoelastic solids. In particular, we will compare the numerical results with the predictions of the (more general) Persson's contact mechanics theory. We use a recently developed residuals molecular dynamics (RMD [11, 12]) scheme, adapted to the rubber viscoelastic rheology. The RMD method has so far has been successfully applied to the investigation of adhesive contacts between elastic solids with random roughness [12], and here we extend the study to the case of sliding contact between linear viscoelastic solids with random surface roughness (see appendix A). The RMD numerical model is based on a (finite element) formulation in wavevector space, together with a molecular dynamics modeling of the interfacial separation in real space, the latter driven by the residuals of the discretized contact mechanics equations. This (general-purpose) approach allows for an equally efficient computation of the contact dynamics from very small values of contact areas up to full contact interactions.

The paper is outlined as follows. In section 2 we summarise the mean field theory of viscoelastic contact mechanics. In section 3 the analytical friction and contact area predictions are compared with the results of RMD simulations, and the existence of an universal contact area law is presented and discussed. Finally, in appendix A the RMD model is briefly described, whereas in appendix B the role of finite size effects on the reported friction and contact mechanics is discussed.

2. Theory

One of us [5] has derived a set of equations describing the friction force acting on a rubber block sliding at the velocity $v(t)$ in contact with a hard substrate with randomly rough surface. For a rubber in dry contact with a hard solid with a rough surface there are two main contributions to rubber friction, namely (i) a contribution derived from the energy dissipation inside the rubber due to the pulsating deformations it is exposed to during sliding (it could be named micro-rolling friction, as it shares the dissipation mechanism with the classical rolling friction), and (ii) a contribution from the shearing processes occurring in the area of real contact. For sliding at a constant velocity v, and neglecting frictional heating (constant bulk temperature), the friction coefficient due to process (i) is:

$$\mu \approx \frac{1}{2}\int_{q_0}^{q_1} \mathrm{d}q\; q^3\, C(q)S(q)P(q) \times \int_0^{2\pi} \mathrm{d}\phi\, \cos\phi\, \mathrm{Im}\frac{E(qv\cos\phi)}{(1-\nu^2)\sigma_0}, \quad (1)$$

where σ_0 is the nominal contact stress, $C(q)$ the surface roughness power spectrum and $E(\omega)$ the rubber viscoelastic modulus. The function $P(q) = A(\zeta)/A_0$ is the relative contact area when the interface is observed at the magnification $\zeta = q/q_0$, where q_0 is the smallest (relevant) roughness wave vector. We have

$$P(q) = \frac{2}{\pi}\int_0^{\infty} \mathrm{d}x\, \frac{\sin x}{x} \exp\left[-x^2 G(q)\right] = \mathrm{erf}\left(\frac{1}{2\sqrt{G}}\right), \quad (2)$$

where

$$G(q) = \frac{1}{8}\int_{q_0}^{q} \mathrm{d}q\; q^3 C(q) \int_0^{2\pi} \mathrm{d}\phi\, \left|\frac{E(qv\cos\phi)}{(1-\nu^2)\sigma_0}\right|^2. \quad (3)$$

The factor $S(q)$ in (1) is a correction factor which takes into account that the asperity-induced deformations of the rubber are smaller than would be in the case if complete contact would occur in the (apparent) contact areas observed at the magnification ζ. For contact between elastic solids this factor reduces the elastic asperity-induced deformation energy, and including this factor gives a distribution of interfacial separation in good agreement with experiment and numerical studies [13]. The interfacial separation describes how an elastic (or viscoelastic) solid deforms and penetrates into the roughness valleys, and it is stressed here that these (time-dependent) deformations cause the viscoelastic contribution to rubber friction. We assume that the same $S(q)$ reduction factor as found for elastic contact is valid also for sliding contact involving viscoelastic solids. For elastic solids it has been found that $S(q)$ is well approximated by

$$S(q) = \gamma + (1-\gamma)P^2(q),$$

where $\gamma \approx 1/2$, and here we use the same expression for viscoelastic solids, being in nature a geometrical parameter. Note that $S \to 1$ as $P \to 1$ which is an exact result for complete contact. In fact, for complete contact the expression (1) is exact (see below). Note finally that in the original rubber friction theory [5] the correction factor $S(q)$ was not included.

The second contribution (ii) to the rubber friction force, associated with the area of (apparent) contact observed at the magnification $\zeta_1 = q_1/q_0$, is given by $\tau_f A_1$. Here, $\tau_f(v)$ is the (weakly) velocity-dependent effective frictional shear stress acting in the contact area $A_1 = A(\zeta_1) = P(q_1)A_0$. In this study we only consider the viscoelastic contribution to the rubber friction, but we also study the area of real contact which is needed when calculating the second contribution to the rubber friction.

Note that the surface mean square slope is given by

$$\left\langle (\nabla h)^2 \right\rangle = 2\pi \int_{q_0}^{q_1} \mathrm{d}q\; q^3 C(q)$$

so we can write

$$\frac{\mu}{\left\langle (\nabla h)^2 \right\rangle} \approx \frac{\int_{q_0}^{q_1} \mathrm{d}q\; q^3 C(q)\, S(q)\, P(q) \int_0^{2\pi} \mathrm{d}\phi\, \cos\phi\, \mathrm{Im}\frac{E(qv\cos\phi)}{(1-\nu^2)\sigma_0}}{4\pi \int_{q_0}^{q_1} \mathrm{d}q\; q^3 C(q)}. \quad (4)$$

For complete contact $S(q) = P(q) = 1$ and if $\mathrm{Im}E(\omega)$ would be weakly dependent on ω, the integral over ϕ in (4) would be weakly dependent on q, and in this limiting case the viscoelastic friction coefficient would be nearly proportional to the mean square slope. However, these assumptions never hold in practice and the friction coefficient cannot be simply related to the mean surface slope [14].

3. Results and discussion

We now present numerical simulations results for the viscoelastic contribution to the friction for a wide range of contact conditions, including nominal contact pressure, sliding velocity, and the large frequency cut-off q_1 (which determines the length scales over which the surface exhibits roughness). The RMD numerical results will be compared with the predictions of the rubber friction theory presented above.

In the calculations we use the viscoelastic modulus $E(\omega)$ measured for a tread rubber compound [15], and the substrate

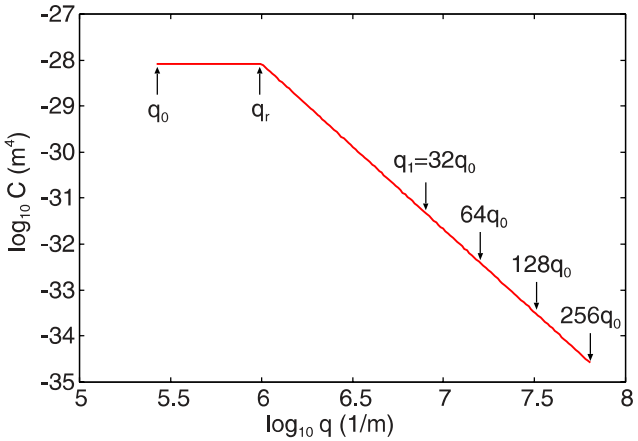

Figure 1. Surface roughness power spectra used in the present study. The power spectra have a low frequency cut-off for $q_0 = 0.25 \times 10^6\,\mathrm{m}^{-1}$, and a roll-off for $q_\mathrm{r} = 4q_0$. For $q > q_\mathrm{r}$ the power spectra correspond to a self-affine fractal surface with the Hurst exponent $H = 0.8$. We consider 4 cases where the large frequency cut-off is $q_1 = 32q_0$, $64q_0$, $128q_0$ and $256q_0$; we refer to $q_1 = 32q_0$ and $256q_0$ as the small and large system, respectively. In the numerical calculations, a null power spectrum region is added between q_1 and $\bar{q}_1 = 8q_1$ to improve convergence.

is assumed rigid with a randomly rough surface with isotropic statistical properties. Figure 1 shows the surface roughness power spectra used in the present study. The power spectra have a low frequency cut-off for $q_0 = 0.25 \times 10^6\,\mathrm{m}^{-1}$, and a roll-off for $q_\mathrm{r} = 4q_0$. For $q > q_\mathrm{r}$ the power spectra correspond to a self-affine fractal surfaces with the Hurst exponent $H = 0.8$. We consider four cases where the large frequency cut-off is $q_1 = 32q_0$, $64q_0$, $128q_0$ and $256q_0$; we refer to $q_1 = 32q_0$ and $256q_0$ as the small and large system, respectively. The root mean square roughness is determined mainly by the long-wavelength roughness and is therefore nearly the same for all the different cases, with $h_\mathrm{rms} \approx 27\,\mathrm{nm}$.

Figures 2(a) and (b) show the friction coefficients (divided by the mean square (ms) slope), as a function of the (normalized) area of contact A/A_0, for the large and small systems, respectively, and for several sliding speeds: $v = 0.01$, 0.1, 1, $10\,\mathrm{m\,s}^{-1}$. The solid lines are the predictions of the Persson's rubber friction theory, whereas the dashed lines are from the numerical study. Note that because of the Hertzian-like contact for small load, the numerical friction curves show a non-monotonic behavior, where friction increases at small increasing values of contact areas (see appendix B for a detailed discussion of finite size effects). For high enough loads the friction coefficient decreases with increasing load (corresponding to increasing contact area) and the numerical results smoothly converge to the mean field predictions. Note that at $A/A_0 \approx 0.05$, the small system is still in the Hertzian friction regime [16], whereas the large system is experiencing the transition. Figure 3(a) and (b) show the contact morphology for $A/A_0 \approx 0.05$ for both the large and small systems, respectively, at sliding speed $v_0 = 10\,\mathrm{m\,s}^{-1}$. For the large system the contact is split in a huge number of smaller patches (compared to the small system). When the surface exhibits roughness at shorter and shorter length scales (i.e. when the cut-off q_1 increases) the Hertzian-like

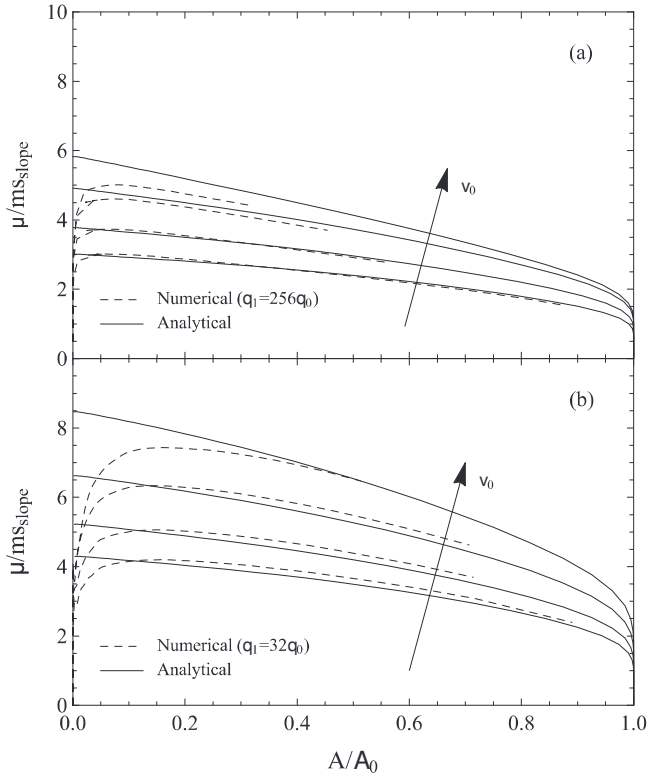

Figure 2. The friction coefficient, divided by the ms slope, as a function of the (normalized) area of contact A/A_0, for several sliding speeds: $v = 0.01$, 0.1, 1, $10\,\mathrm{m\,s}^{-1}$. The solid lines are the theory predictions, while the dotted lines are from the numerical simulations. For (a) large system, and (b) small system.

contact will prevail only at lower and lower nominal contact pressure, i.e. the finite size effect will be confined at smaller nominal contact areas and the system will move toward the thermodynamic limit, where a remarkably good agreement with the mean field theory exists (the interested reader is remanded to [17] for a detailed study of finite size effects on the elastic roughness contact mechanics).

Figure 4 shows the (normalized) area of real contact as a function of the applied pressure p_N [divided by the root mean square (rms) slope], for several values of roughness cut-off frequencies ($q_1 = 32q_0$, $64q_0$, $128q_0$ and $256q_0$) and sliding velocities ($v = 1$, $10\,\mathrm{m\,s}^{-1}$). In particular, the solid lines are the theory results and the dotted lines are from the numerical simulations. The agreement is very good, even at small contact areas (see appendix B). It is observed that when the sliding velocity increases, the asperity deformation frequencies increase and the rubber becomes elastically stiffer, resulting in the decrease of the contact area with increasing sliding speed. Moreover, this local stiffening depends on the perturbing frequencies which increases when more short-wavelength roughness is added to the surface profile, i.e. when q_1 increases. Therefore, for viscoelastic contacts one cannot expect the area of real contact to be proportional to the inverse of the the root-mean-square roughness as observed for elastic contacts. This is confirmed by figure 4 which shows that for each velocity value, the numerically-predicted curves are not superposing, in agreement with the analytical results (2).

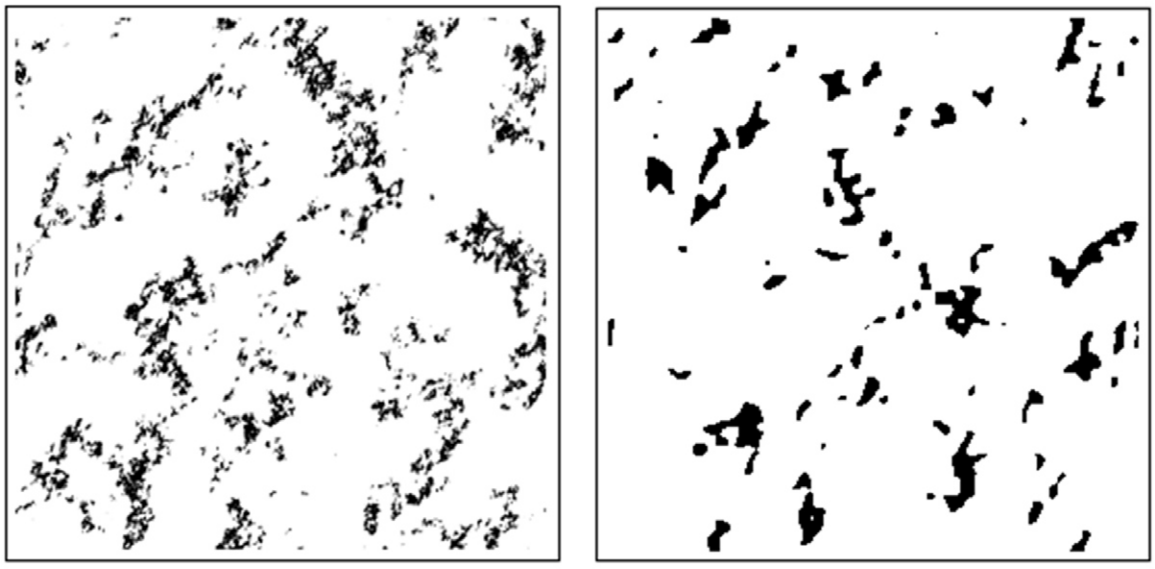

Figure 3. The contact morphology for the sliding speed $v = 10\,\mathrm{m\,s^{-1}}$ and for such a normal load that $A/A_0 \approx 0.05$. (a) large system, (b) small system. Black domains correspond to the true contact area. The sliding direction is from left to right.

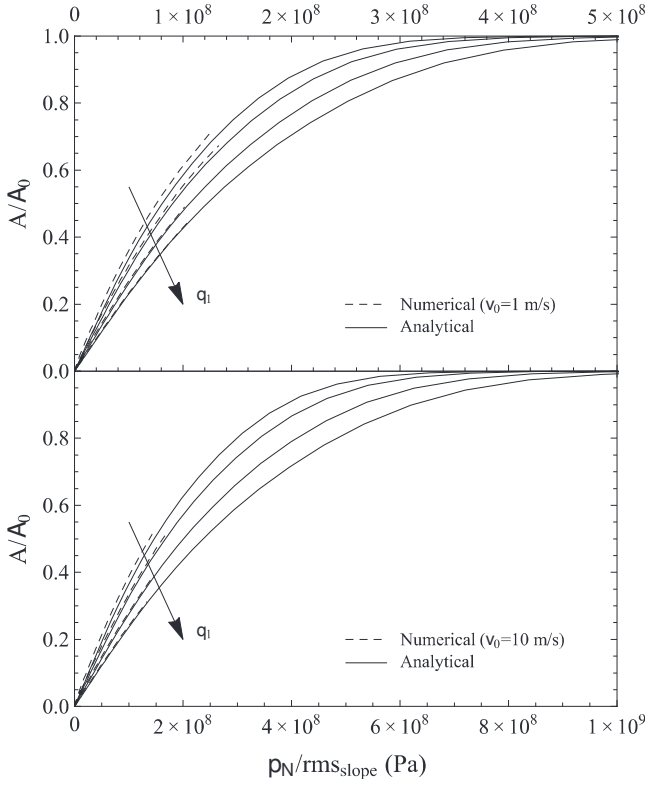

Figure 4. The normalized area of contact A/A_0 as a function of the contact pressure p_N (divided by the rms slope), for several large cut-off frequencies q_1. The reported values correspond to sliding velocities occurring in the rubbery-to-glassy rubber transition regime.

However, the analytical theory (2) and (3) suggests a possible mechanism to interpret the contact area results. As shown in equation (3), this local (scale dependent) rubber stiffening is equivalent to an apparent increase (with respect to the static contact) of the roughness power spectral content by a factor

$$s\,(q,\,v_0) = \frac{1}{2\pi}\int_0^{2\pi} \mathrm{d}\phi\,\left|\frac{E\,(q\,v\,\cos\phi)}{E_0}\right|^2, \tag{5}$$

where E_0 is the low frequency rubber elastic modulus [$E_0 = E(\omega \to 0)$]. Hence, it is now easy to define a new (viscoelastic-dependent) effective mean square slope as

$$\left\langle(\nabla h)^2\right\rangle_E = 2\pi\int_{q_0}^{q_1} \mathrm{d}q\; q^3 C\,(q)\,s\,(q,\,v)\,, \tag{6}$$

which is depending on the sliding velocity v via the dependency of $E(\omega)$ on $\omega = q\,v\cos\phi$. In figure 5 we shown the normalized contact area as a function of the contact pressure scaled by the effective root mean square slope, for several values of roughness cut-off frequencies ($q_1 = 32q_0$, $64q_0$, $128q_0$ and $256q_0$) and sliding velocities ($v = 0.01,\ 0.1,\ 1,\ 10\,\mathrm{m\,s^{-1}}$). Remarkably, the theory-suggested scaling allows to obtain an unique contact mastercurve similar to the case of purely elastic interactions, with a slope close to two as also observed for elastic contact. Hence, it is recognizable that an universal scaling rules the asperity mediated multiscale interaction of randomly rough surfaces, which is insensitive to the particular rheological description of the bulk dynamics.

4. Conclusions

We have performed numerically-exact calculations for the viscoelastic contribution to rubber friction, and compared the results with the prediction of an analytical theory. Both the friction coefficient and the area of contact are rather well described by the theory, in particular for large contact pressure

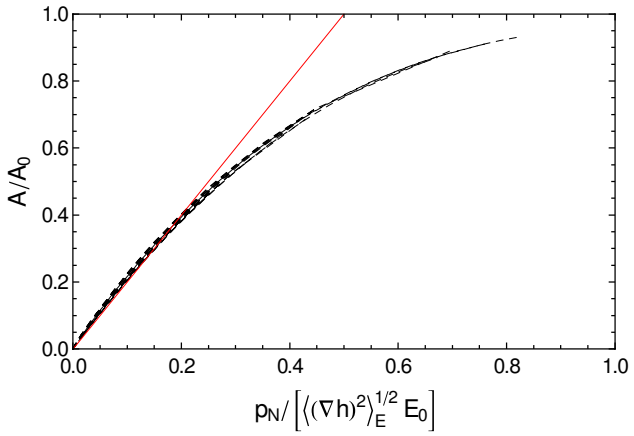

Figure 5. The numerically-calculated nominal contact area A/A_0 as a function of the contact pressure $p_N/[\langle(\nabla h)^2\rangle_E^{1/2} E_0]$ [where $\langle(\nabla h)^2\rangle_E^{1/2}$ is an effective mean-square surface slope defined in (6)], for several values of roughness cut-off frequencies ($q_1 = 32q_0$, $64q_0$, $128q_0$ and $256q_0$) and sliding velocities ($v = 0.01$, 0.1, 1, 10 m s^{-1}). All the curves appear superposed to an unique mastercurve. The red line has a slope of 2.

(in the limit of complete contact, the analytical theory is exact). Viscoelasticity will introduce some anisotropy in the contact morphology, but this effect seems to be rather unimportant for the variation of the rubber friction and contact area with sliding speed. In the numerical calculations we have neglected the effect of frictional heating and strain softening, which are likely to be important in most practical applications. These effects can be approximately included in the analytical theory, but including the same effects in the numerically exact treatment seams highly non-trivial.

Acknowledgments

MS acknowledges FZJ for the support and the kind hospitality received during his visit to the PGI-1, where this work was initiated. MS also acknowledges COST Action MP1303 for grant STSM-MP1303-090314-042252.

The research work was performed within a Reinhart-Koselleck project funded by the Deutsche Forschungsgemeinschaft (DFG). The authors would like to thank DFG for the project support under the reference German Research Foundation DFG-Grant: MU 1225/36-1.

Appendix A. Numerical model

Here we summarize the numerical model discussed in detail in [11]. We consider the case of two viscoelastic solids patterned with random or deterministic roughness. We assume the generic roughness to be characterized by a small wavelength cut-off $q_0 = 2\pi/L_0$ with $L_0 \ll L$, where L is the representative size of the macroscopic contact region between the two solids. Given such a large difference of length scales, we can easily identify a representative elementary volume (RVE) of interface of length scale L_{RVE}, with $L_0 \ll L_{\mathrm{RVE}} \ll L$, over which we can average out the contact mechanics occurring at smaller length scales (say, at $\lambda \ll L_{\mathrm{RVE}}$).

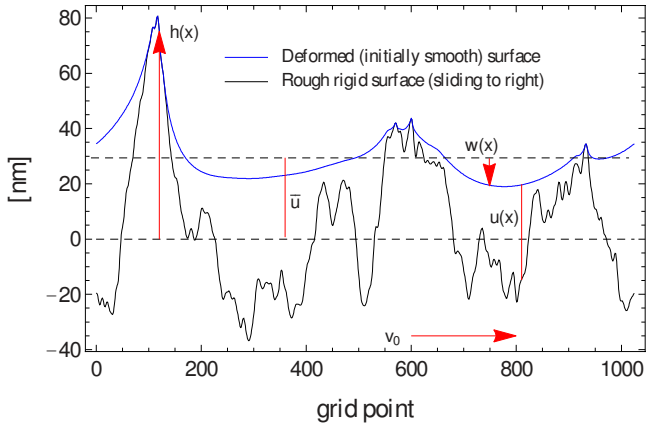

Figure A1. Description of the gap [see equation (A.1)] resulting from a generic cross section of the contact interface. v_0 is the sliding velocity.

In figure A1 we show a schematic of the contact geometry. We assume the contact to occur under isothermal conditions, and the roughness to be characterized by a small mean square slope, in order to make use of the well-known half-space theory. Moreover, the roughness is assumed to be periodic with period L_0 in both x- and y-direction. The local separation between the mating interfaces u (x) is shown in figure A1, and it can be immediately agreed to be:

$$u\,(\mathrm{x}) = \bar{u} + w\,(\mathrm{x}) - h\,(\mathrm{x})\,, \tag{A.1}$$

where $\bar{u}$ is the average interfacial separation, w (x) the surface out-of-average-plane displacement and h (x) the surface roughness, with $\langle w\,(\mathrm{x})\rangle = \langle h\,(\mathrm{x})\rangle = 0$. By defining

$$w\,(\mathrm{q}) = (2\pi)^{-2} \int \mathrm{d}^2\mathrm{x}\; w\,(\mathrm{x})\, \mathrm{e}^{-\mathrm{i}\mathrm{q}\cdot\mathrm{x}}$$

and

$$\sigma\,(\mathrm{q}) = (2\pi)^{-2} \int \mathrm{d}^2\mathrm{x}\; \sigma\,(\mathrm{x})\, \mathrm{e}^{-\mathrm{i}\mathrm{q}\cdot\mathrm{x}},$$

where σ (x) is the distribution of interfacial pressures, it is (relatively) easy to show that w (x) can be related to σ (x) through a very simple equation in the Fourier space:

$$w\,(\mathrm{q}) = F\,(\mathrm{q})\, M_{zz}\,(\mathrm{q})\, \sigma\,(\mathrm{q})\,, \tag{A.2}$$

where $M_{zz}\,(\mathrm{q}) = -2/\left[|\mathrm{q}|\, E_r\,(\mathrm{q}\cdot \mathrm{v}_0)\right]$ for the viscoelastic half space [$M_{zz}\,(\mathrm{q})$ is also known analytically for layered materials], $E_r\,(\omega)$ is the frequency-dependent (complex) reduced Young's modulus, v_0 is the sliding velocity and $F\,(\mathrm{q})$ is the Fourier transform of the real space linear shape function [11]. The viscoelastic modulus can be measured recurring to standard techniques [18], and its real and imaginary part fitted by Prony series [19], obtaining e.g.:

$$\frac{1}{E_r(\omega)} \approx \frac{1}{E_r(\infty)} + \sum_{n=1}^{N} \frac{H_r(\tau_n)}{1 - \mathrm{i}\omega\tau_n},$$

where N is the number of relaxation times, $H_r(\tau_\mathrm{n})$ the discrete creep function, and τ_n the relaxation time. $E_r(\infty)$ is the (asymptotic) reduced elastic modulus in the rubber glassy

region. We stress that the distribution of relaxation times (describing real rubber rheologies) is very wide, and cannot be characterized by a simple single relaxation time as often assumed in the literature.

Finally, the relation between separation u (x) and interaction pressure σ (x) is calculated within the Derjaguin's approximation [12], and it can be written in term of a generic interaction law

$$\sigma\left(u\right) = f\left(u\right). \tag{A.3}$$

$f\left(u\right)$ will be repulsive for u □ u_{w} and attractive otherwise, where u_{w} is a separation threshold describing the ideal equilibrium separation. In this work we have only adopted the repulsive term of the L–J potential, but one can equally make use of the entire law, as well as of different interaction laws (e.g. the Morse potential, for chemical bonds).

Equations (A.1) and (A.3) are discretized on a regular square mesh of grid size δ, resulting in the following set of equations:

$$L_{ij} = -u_{ij} + \left(\bar{u} + w_{ij} - h_{ij}\right) \tag{A.4}$$

$$\sigma_{ij} = f\left(u_{ij}\right) \tag{A.5}$$

$$\sigma\left(x_{ij}\right) \rightarrow \Delta\sigma\left(q_{hk}\right) = F^{-1}M_{zz}^{-1}w\left(q_{hk}\right) \rightarrow w\left(x_{ij}\right), \tag{A.6}$$

where L_{ij} is the generic residual (related to the generic iterative solution u_{ij}). In order to solve equations (A.4)–(A.6), we rephrase equation (A.4) in terms of the following ideal molecular dynamics process

$$\ddot{u}_{ij} + 2\xi_{ij}\omega_{ij}\dot{u}_{ij} = \omega_{ij}^2 L_{ij}, \tag{A.7}$$

which we solve with a velocity Verlet integration scheme. ξ_{ij} and ω_{ij} are, respectively, the generic damping factor and modal frequency of the residuals molecular dynamics system (RMD), which can be used to damp the error dynamics. Therefore, at equilibrium ($\ddot{u}_{ij} = \dot{u}_{ij} = 0$), equation (A.7) returns the solution of equations (A.4)–(A.6) at zero residuals. The solution accuracy is set by requiring

$$\left\langle L_{ij}^2/u_{ij}^2\right\rangle^{1/2} < \varepsilon_{\mathrm{L}}; \left\langle\left[\left(u_{ij}^n - u_{ij}^{n-1}\right)/u_{ij}^{n-1}\right]^2\right\rangle^{1/2} < \varepsilon_{\mathrm{u}}, \tag{A.8}$$

where both errors are typically of order 10^{-4}.

Appendix B. Finite size effects on friction

It is interesting to note that while we observe a negligible finite-size effect for the contact area, the numerically obtained friction coefficient rapidly drops as the nominal contact pressure approaches to zero. We can explain this as follows: Finite size effects are important when the long-wavelength roughness strongly influences the quantity under consideration. The long-wavelength roughness is different in the analytical and numerical model. Thus, while in the wavevector region where $C(q)$ is non-vanishing the analytical model has the same (finite) power spectrum as in the numerical model, the latter is for a small system of linear size $2\pi/q_0$, whereas the former is for an infinite system. This implies that in the analytical model, beyond the roll-off (or cut-off) region, the power spectrum has a region with $C(q) = 0$ extending down to $q = 0$ (which correspond to an infinite system as the lower cut-off frequency $q = 2\pi/L$, where $L = \infty$ is the linear size of the system). For an infinite system with Gaussian random roughness, as assumed in the analytical (and approximated in the numerical) model, there will be infinite high asperities, and contact between two solids will occur for any arbitrary large separation. However, the numerical model is for a finite sized system, and all asperities will be of a finite height. Clearly in this case the contact mechanics involving the long-wavelength roughness components may be rather different in the analytical and numerical models. Only by adding a large enough wavelength region for $q < q_0$ (where $C(q) = 0$) in the numerical model the latter will approach the corresponding system used in the analytical study.

Moreover, we stress that (in the analytical contact mechanics theory [5]) the contact area depends on the function $G(q)$, the integrand of which scales as $q^3C(q) \sim q^{1-2H}$. If we use a logarithmic q-scale, $\mu = \log(q/q_0)$, the integrand scales as q^{2-2H}. Thus if $H = 1$ all decades in length scale are equally important for the contact area, and since the small wavevector part of the μ-integral, which is influenced by the system finite size (e.g. the size of the roll-off region) is a small fraction of the total μ-integration interval, the contact area will exhibit very small finite size behaviours as indeed observed. Now in the friction integral, in addition to the same q-factor $[q^3C(q)]$ as in the integral for the contact area, two additional q-dependent factors enter, namely from the E-modulus and from $P(q)$. For small nominal contact pressures $P(q)$ very rapidly drops from ≈ 1 at $q = q_0$ (or $\zeta = 1$ or $\mu = 0$), to a very small value for $q \gg q_0$. This implies that the rubber friction for very small nominal contact pressures depends strongly on the very long-wavelength roughness, and this results in the observed finite size effects. Similar arguments can be given for the contact stiffness, which for small nominal contact pressures also depends mainly on the long-wavelength roughness.

We finally observe that the fact that the rubber friction for very small nominal contact pressures mainly depends on the very long-wavelength roughness implies that, for a small system, the contact can be considered to occur between one or a few high asperities with smooth surfaces. For a Hertzian-like contact one can show that the friction coefficient vanishes linearly with the average pressure $\sigma = F_{\mathrm{N}}/A$ acting in the contact region[3], therefore (for a Hertzian contact where $A \sim F^{2/3}$) the friction coefficient vanishes as $\sim F^{1/3} \sim A^{1/2}$ as $A \rightarrow 0$. The analytical theory is for an infinite system and in this case there will always be infinite many contact regions and the area of real contact will be proportional to the normal force, resulting in a friction coefficient independent of the load (or contact area) as the load goes to zero.

[3] See, e.g. equation (19) in Persson [20]. This reference is for rolling friction but the same result prevails for the sliding friction when no frictional shear stress acts in the contact regions, as assumed in this study.

References

[1] Grosch K A 1963 *Proc. R. Soc. Lond. Ser.* A 274 21
[2] Schallamach A 1963 *Wear* 6 375–82
[3] Ludema K C and Tabor D 1966 *Wear* 9 329–48
[4] Ferry J D 1980 *Viscoelastic Properties of Polymers* 3rd edn (New York: Wiley)
[5] Persson B N J 2001 *J. Chem. Phys.* 115 3840
[6] Persson B N J, Albohr O, Tartaglino U, Volokitin A I and Tosatti E 2005 *J. Phys.: Condens. Matter* 17 R1–62
[7] Hyun S, Pei L, Molinari J-F and Robbins M O 2004 *Phys. Rev.* E 70 026117
[8] Carbone G and Putignano C 2014 *Phys. Rev.* E 89 032408
[9] Carbone G and Putignano C 2013 *J. Mech. Phys. Solids* 61 1822
[10] Klüppel M and Heinrich G 2000 *Rubber Chem. Technol.* 73 578
[11] Scaraggi M 2015 in preparation
[12] Persson B N J and Scaraggi M 2014 *J. Chem. Phys.* 141 124701
[13] Almqvist A, Campana C, Prodanov N and Persson B N J 2011 *J. Mech. Phys. Solids* 59 2355
[14] Li Q, Popov M, Dimaki A, Filippov A E, Kurschner S and Popov V L 2013 *Phys. Rev. Lett.* 111 034301
Lyashenko I A, Pastewka L, and Persson B N J 2013 *Phys. Rev. Lett.* 111 189401
[15] Lorenz B and Persson B N J 2014 unpublished
[16] Greenwood J and Tabor D 1958 *J. Phys. Soc.* 71 989
[17] Pastewka L, Prodanov N, Lorenz B, Müser M H, Robbins M O and Persson B N J 2013 *Phys. Rev.* E 87 062809
[18] Lorenz B, Pyckhout-Hintzen W and Persson B N J 2014 *Polymer* 55 565–71
[19] Scaraggi M and Persson B N J 2014 *Tribiol. Lett.* 55 15–21
[20] Persson B N J 2010 *Eur. Phys. J.* E 33 327